16th World Conference on Earthquake, 16WCEE 2017

Santiago Chile, January 9th to 13th 2017

Paper N°3662

Registration Code: S-Q1462718155

SHAKING TABLE TESTS ON SEISMIC FAILURE MECHANISM OF ELEVATED-PILE-FOUNDATION-SUPPORTED BRIDGES IN LIQUEFIED OR NONLIQUEFIABLE SOIL

X. Wang [1], Y. Shang [2], A. Ye [3]

[1] *Ph.D. Candidate, State Key Laboratory of Disaster Reduction in Civil Engineering, Tongji University, 10_xiaoweiwang@tongji.edu.cn*
[2] *Ph.D. Candidate, State Key Laboratory of Disaster Reduction in Civil Engineering, Tongji University, 0725shangyu@tongji.edu.cn*
[3] *Professor, Ph.D., State Key Laboratory of Disaster Reduction in Civil Engineering, Tongji University, yeaijun@tongji.edu.cn (corresponding author).*

Abstract

One-g shake-table experiments are conducted to explore the seismic failure mechanism of bridges supported by elevated pile foundation embedded into liquefiable or nonliquefiable soil. Two identical specimens consist of 2*2 reinforced concrete (RC) pile group, RC cap and single RC pier were constructed and embedded into saturated and dry sand, respectively. A lumped iron block was assigned at the pier top to represent the superstructure. Scaled Kobe and Chichi ground motions were adopted as seismic inputs. Representative test data, including frequency and damping properties of the soil-structure system, time histories of excess pore pressure ratios and accelerations, and curvature distributions along the piles are presented. Test results indicate a strong effects of soil liquefaction on the seismic failure mechanism of elevated-pile-foundation-supported bridge structures. Under strong seismic excitation, two plastic regions were formed on pile head and underground successively for the specimen in liquefiable soil. By contrast, the plastic region below the soil surface was formed first for the specimen in nonliquefiable soil. Besides, the specimen in liquefiable sand displays a deeper depth of underground plastic region than that in the nonliquefiable sand. Quantitative analysis results from recorded data coincide reasonably well with the post-shaking observation of pile damages.

Keywords: Bridge structure; shaking table test; seismic failure mechanism; soil liquefaction; riverbed scour.

1. Introduction

For river-crossing bridges, foundations are usually constructed in deep water and embedded into soil. Saturated soil may liquefy under seismic excitation, leading to reductions of soil resistance, which may cause the damage of pile foundations and further the failure of bridge structures. Although arduous efforts have been made in past decades to reveal the seismic behavior of pile-supported bridge structures in liquefiable soil, recent earthquake disasters [1,2] still show the lack of knowledge on this issue, especially the unclearness on the complex seismic failure mechanism. Meanwhile, pile foundations constructed in deep water are usually suffered to riverbed scour, which is reported to be one of the most severe hazards that cause bridge failure in the United States [3]. Specifically, scour may render the cap and upper portion of the piles exposed without surrounding soil, forming the so called *elevated pile foundation* [4], which results in a capacity degradation of the foundation and alters the dynamic behavior of bridge structures under seismic hazard [5]. A brief introduction of previous representative test studies on pile-supported structures in liquefiable or scour scenarios follows.

Previous studies mainly focused on the seismic behavior of piles and pile-supported structures in liquefiable soil alone. Many attempts have been made through centrifuge tests [6–8], shaking table tests [9,10], and in-situ blast tests [11,12]. As to experimental studies in bridge scour field, rare related work has been reported. Wang et al. [13] investigated the seismic performance of a scoured pile-supported bridge model embedded into dry sand using shaking table tests and found that with the increase of scoured depth, the potential failure mechanism transferred from the pier to the pile foundation. In practice, it is common scenario that bridges located at perennial flood-induced scour sites where saturated sand may liquefy during earthquakes. However, experimental studies on seismic behavior of pile-supported bridge structures in combination of scour and earthquake-induced liquefaction hazards have rarely been documented to the authors' knowledge. In these regards, it is critical to investigate the seismic failure mechanism of bridge structures in both liquefiable and scour scenarios.

A key objective of this study is to reveal the seismic failure mechanism of pile-supported bridge structures in liquefiable soil under riverbed scour scenario. To this end, a shaking table test under scaled earthquake motions was performed on a simplified RC bridge model partially embedded into fully saturated sand. For comparison, another shaking table test on an identical bridge model in dry sand with the same scour depth and very close relative density (D_r) was carried out to clarify the impact of soil liquefaction on its seismic response and failure mechanism. Soil response of acceleration and pore water pressure were presented. Recorded pile curvature distributions were illustrated to reveal the seismic failure mechanism, which was then related to the post-test physical observation of the damaged models. This study serves as a complement to the research on inelastic behavior of piles by documenting the demands of actual RC pile-supported bridge structures in idealized homogenous soil profiles.

2. Test Setup and Instrumentation

A series of shaking table tests were carried out at the Multi-functional Shaking Table Lab of Tongji University, Shanghai (Fig. 1). A laminar soil box with inside dimensions of 2 m×1.5 m×2 m (length×width×height) was mounted on the 4×6 m shaking table with maximum bearing capacity of 70 ton. As schematized in Fig. 2, two identical RC specimen composed of a 1.9 m-length/0.1 m-diameter (D) 2×2 pile group and a 0.6 m×0.6 m×0.3 m cap and a 1.0 m-height/0.214 m-diameter single pier were constructed and partially embedded into, separately, saturated or dry sand with similar D_r around 50% and the same scour depth of 0.4 m. A 4 ton iron block was fixed on the top of the pier as the superstructure.

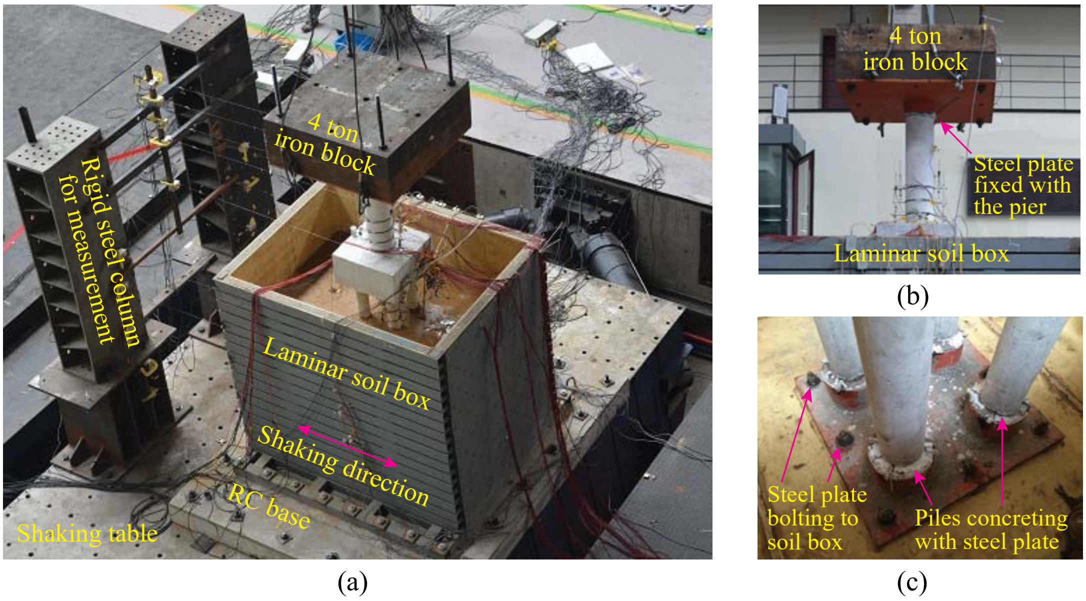

Fig. 1 – Test specimen embedded in laminar soil box on the shake table at the Multi-functional Shaking Table Lab of Tongji University: (a) global view, (b) pier-superstructure connection and (c) pile-tip connection.

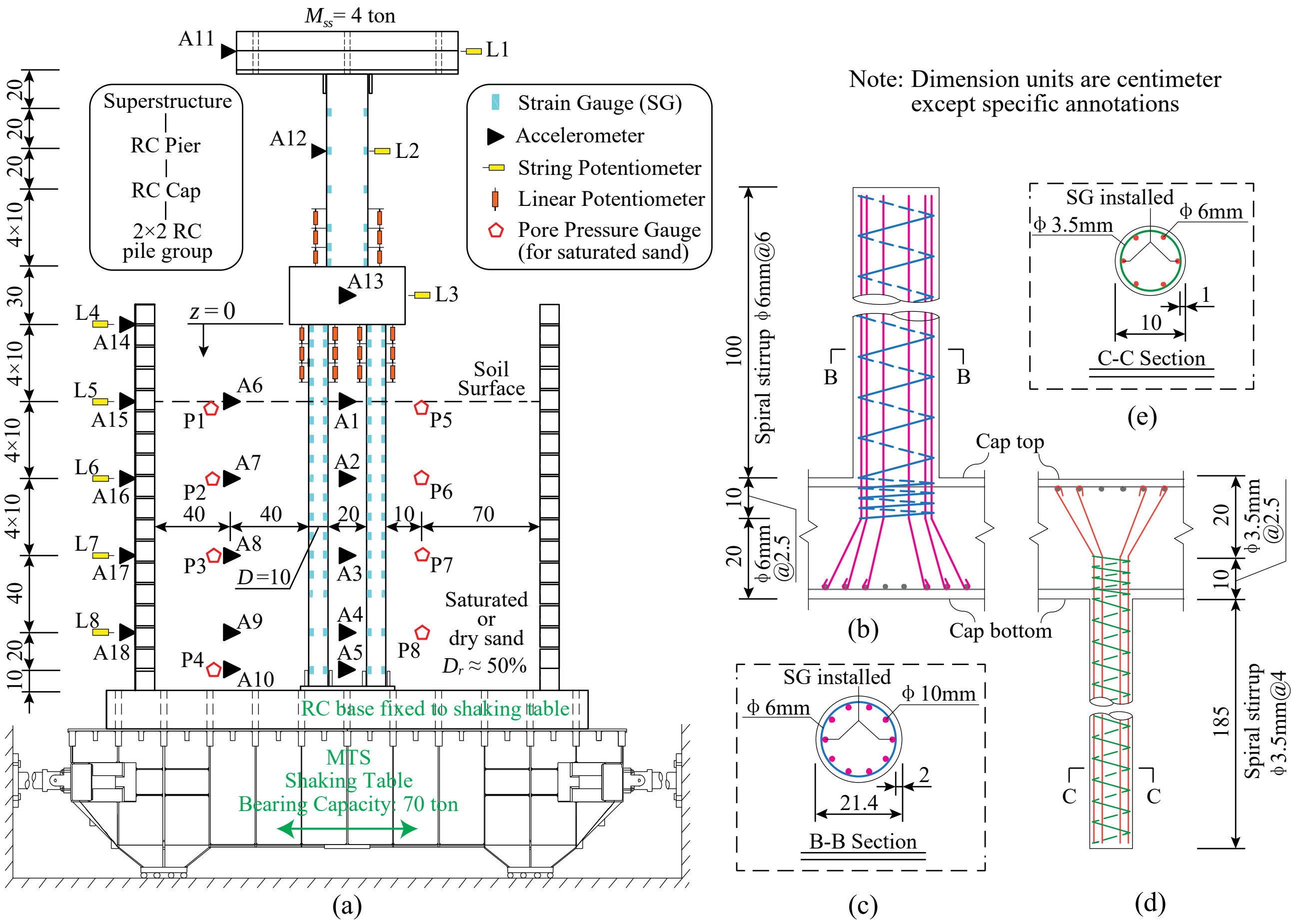

Fig. 2 – Bridge specimen in saturated or dry medium dense sand for shaking table tests: (a) global schematic diagram, (b) pier reinforcement, (c) pier section, (d) pile reinforcement and (e) pile section

2.1. Bridge Model Property

One novel point of this experimental study is the comprehensive consideration of a soil-bridge system; that is the soil-pile-cap-pier-superstructure model, not only the piles as many previous studies did. In this regard, the predominant period of an ordinary bridge structure was taken as the criteria during the design of the test specimens. AASHTO LRFD Bridge Design Specifications [14] indicated that 0.2 and 1.0 s are usually supposed to be the short and long predominant periods for ordinary multi-span girder bridges. Thus, in this study, a predominant period of 0.4 ~ 0.5 s was considered when designing the specimens. To this end, a value of lumped mass (M_{ss} = 4 ton) is chosen to meet the target of expected predominant period of the specimen as well as the axial compressive ratio of bridge columns in current practices (i.e., between 5% and 35%) [15].

Four piles were connected together by a RC cap in a 2×2 pattern with a center-to-center spacing of 3*D*. This value was chosen based on current practices that commonly adopts a spacing of 3*D* to 4*D* [16]. As seen in Fig. 1(b), the pier head is fixed with the lumped mass through a steel plate with a collar, which was casted together with the pier by welding the top of the reinforcing rebar to the steel plate. In terms of the pile-tip and base connection (Fig. 1(c)), a 4-collar steel plate was casted together with the 2×2 pile group. It is worth to note that, before casting, the reinforcement cages of the piles just stood in the collars without any other connection. To minimize the boundary effects, the specimen was positioned in the center of the soil box with the distance to the box wall of 8*D* in the shaking direction and 5.5*D* in the orthogonal direction. Details about the reinforcements follows.

A longitudinal and transverse reinforcement ratio of 2% and 0.8% was assigned for the pier and piles of the specimen, respectively. Specifically, as shown in Fig. 2, for the pier component, the longitudinal reinforcements were provided by 10 ϕ10-mm rebars with a concrete cover of 2 cm. In regard to the pier confinement, spiral ϕ6-mm stirrups were arranged with an interval of 6 cm. In addition, longitudinal rebars and dense spiral stirrups were extended into the cap to ensure the fixed connection between the pier and cap top. In terms of the pile components, 6 ϕ6-mm rebars were assembled as longitudinal reinforcements with a cover of 1 cm. The confinements of the pile is supplied with spiral ϕ3.5-mm stirrups with an interval of 4 cm. Similarly, dense spiral stirrups were extended to the cap to guarantee the fixed connection between piles and cap bottom.

Tension tests of the reinforcements indicate that the longitudinal rebars and transverse bars were both characterized by well-defined constitutive relationships. The average compressive strength of the concrete in tests was f_c = 33.7 MPa. Accordingly, section analyses were performed using *OpenSees* [17]. The pier section had a first-yielding curvature of 0.0224 rad/m and the pile section had a larger first-yielding curvature of 0.0380 rad/m.

2.2. Soil Property and Placement

The Shanghai sand was used for the in-place saturated soil layers. The sand is poorly graded, with a mean grain size D_{50} of 0.33 mm, a coefficient of uniformity C_u of 2.06, maximum and minimum dry densities of 1.654 and 1.429 g/cm^3, respectively. To achieve a fully saturated sand layers with D_r of 50%, 20 cm height of pure water was pumped into the box before soil placement. The air pluviation approach was adopted to place the sand into the box. A large steel bucket full of weighted dry sand was suspended over a long hopper. Then, the dry sand was dropped into the water slowly and evenly through the hopper that was just beyond the water surface. After the sand was compacted to a scheduled height, another 10 cm height of water was pumped into the container very slowly. The placement of the next soil layer continued with this procedure. Note that, during the soil placement, the water level kept 5 to 10 cm higher than the soil surface to achieve a fully saturated circumstance. Finally, a total dropped mass of 6823 kg and volume of 4.453 m^2 of dry sand were placed into the laminar container, which corresponds to an average D_r of 49.54%. The placed soil and steel pile were left standing overnight to ensure a stable saturated ground. Before the lateral loading, three samples of the sand were taken randomly from the laminar container and a mean saturated density of 1.785 g/cm^3 was obtained.

As to the nonliquefiable case, dry sand was placed into the container without water. Similar air pluviation approach was used to achieve a D_r close to 50%. Finally, a total dropped mass of 6841 kg and volume of 4.453 m^2 of dry sand were placed into the container, which corresponds to an accumulative D_r of 51.53%. Note that the slight difference of accumulative D_r between the liquefiable and nonliquefiable cases are ignored in this study.

2.3. Test Instrumentation

The laminar soil box and the bridge specimen were instrumented with 132 sensors, including accelerometers, linear potentiometers, string potentiometers, pore pressure transducers (only for liquefiable scenario), and strain gauges. As illustrated in Fig. 2, 10 horizontal accelerometers and 8 pore pressure transducers were embedded in the soil layers in two vertical lines (near piles and far from piles) beyond a distance of 40 cm to the wall of the soil box, which was proved to be far enough to eliminate the boundary effects [18]. Horizontal accelerometers were also installed on the lumped mass and aboveground structures. 40 pairs of strain gauges were glued on representative the longitudinal rebars (shown in Fig. 2) of the pier and two of the four-pile group to monitor the variation of sectional curvature during the test. Because strain gauges were vulnerable in the casting and testing procedures, 9 pairs of linear potentiometers were also adopted at the potential damage regions of the aboveground piles and pier.

2.4. Test Protocol

White noise and amplitude-scaled real ground motions were sequentially applied to the specimens. Table 1 summarizes the adopted ground motions which were original from: (1) the 1999 Chi-chi, Taiwan earthquake (WNT Station, magnitude, M=7.62, source to distance, R=16.27km) and (2) the 1995 Kobe, Japan earthquake (Port Island Station, M=6.9, R=3.31km), as displayed in Fig. 5 (a) and (b), respectively. Apparently, the Chi-chi record contained more cycles of strong shaking than the Kobe motion. Also, as seen their acceleration response spectra in Fig. 3 (c) and (d), these two ground motions contained a quite different frequency content. The Chi-chi wave contained higher frequency contests, corresponding to a maximum amplitude around the period of 0.24 s, whereas the Kobe wave comprised lower frequency contents (i.e., longer predominant period of 1.06 s). Note that, for convenience, the liquefiable scenario (saturated sand) is designated as "L" and the nonliquefiable one (dry sand) is assigned as "N" in tables hereinafter. For the L scenario, an interval duration was adopted among the sequential input motions to ensure the complete dissipation of pore water pressure. Specifically, after the 0.05g white noise for both scenarios, Chi-chi motion with peak input acceleration of 0.1g (Chi-chi 0.1g), Kobe 0.1g and Chi-chi 0.3g was applied to both the L and N scenarios sequentially.

Table 1 – Input ground motions series during the test

Scenario	Motion name	Description	Interval between events for liquefiable scenario (min)
L / N	White noise	0.05g, 0.25~50Hz	N/A
L / N	Chi-chi 0.1g	Scaled to PGA = 0.1g	26
L / N	Kobe 0.1g	Scaled to PGA = 0.1g	35
L / N	Chi-chi 0.3g	Scaled to PGA = 0.3g	30
L (final)	Kobe 0.3g	Scaled to PGA = 0.3g	30
N (final)	Chi-chi 1.0g	Scaled to PGA = 1.0g	/

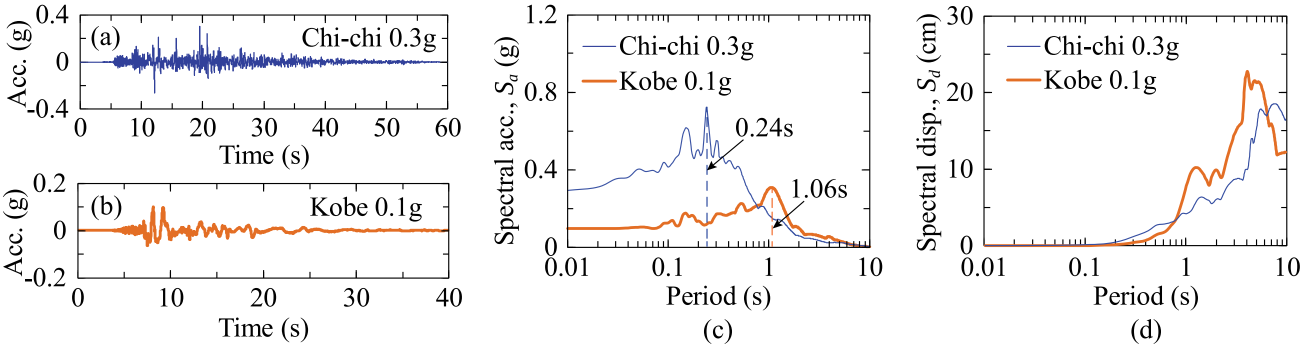

Fig. 3 – Time histories and response spectra of representative input ground motions with damping ratio of 5%: (a) Chi-chi 0.3g, (b) Kobe 0.1g, (c) acceleration and (d) displacement.

3. Results and Interpretation

3.1. Frequency and Damping Features of Soil-Bridge System

The acceleration response of the superstructure and soil in different depths under the 0.05g white noise were adopted to estimate the frequency and damping properties of the soil-bridge structure system. The *Fast Fourier Transform* (FFT) algorithm was first applied to transfer the time history records to frequency spectra. It is noted that from the direct Fourier amplitude, extract well defined peaks are challenging to find. Therefore, the *locally weighted linear regression* algorithm [19] was used to generate a smoothed continuous curve. The damping ratios of the test models were estimated from the width of the resonant peak in the frequency spectrum (smoothed curve) using the *half-power bandwidth method*, which is expressed by the following:

$$\zeta = \frac{f_2 - f_1}{2 f_n} \tag{1}$$

where f_n is the natural frequency, and f_2 and f_1 are the frequencies below and above f_n at which the amplitude is $1/\sqrt{2}$ times the resonant peak.

Table 2 lists the frequencies of bridge models and soil. Note that the structural frequency and damping ratio came from the acceleration response of the superstructure while the soil results was the average value of test data at different depths from A6 to A10. The predominant periods of both bridge model were around 0.5 s, which, as expected, characterizes the dynamic properties of ordinary multi-span girder bridges (0.2 ~ 1.0 s). Also, the liquefiable scenario displayed a slight longer period of both soil and structure than that of the nonliquefiable scenario because very slight liquefaction occurred during the 0.05g white noise excitation. The excess pore water pressure ratio, r_u (i.e., the ratio between the recorded variation of pore water pressure at a depth and the effective overburden stress at that depth) developed to approach 0.2 at a depth of 4*D* to the soil surface. Meanwhile, higher damping ratio was derived from the liquefiable scenario than that from the nonliquefiable scenario. For the soil, a damping ratio of 1.47% in the nonliquefiable scenario increased to 2.28% in the liquefiable scenario due to the effect of soil liquefaction. As to the damping feature of the bridge models, a similar increasing was obtained, from 5.38% in the nonliquefiable scenario to 8.43% in the liquefiable scenario.

Table 2 – Frequency and damping features of the soil and structure from white noise results

Scenario	Predominant frequency (Hz)		Predominant period (s)		Damping ratio (%)	
	Soil	Structure	Soil	Structure	Soil	Structure
L	8.51	1.98	0.12	0.51	2.28	8.43
N	11.44	2.07	0.09	0.48	1.47	5.38

3.2. Soil Pore Water Pressure Development

Fig. 4 shows the time histories of r_u at different depths for the liquefiable scenario. The three locations were at depths of 4*D*, 8*D* and 14*D* to the soil surface, respectively (P2, P3 and P4 in Fig. 2). It is worth to note that the pore pressure gauges at the soil surface (P1 and P5 in Fig. 2) did not show valid data because of the rapid dissipation of pore water pressure at the surface.

In general, the liquefaction extent increased gradually during the sequential input motions. Specifically, a peak r_u of 0.5 was achieved under Chi-chi 0.1g. Both Kobe 0.1g and Chi-chi 0.3g motions triggered significant liquefaction during the test. However, due to the differences on frequency contents of the motions, Chi-chi 0.3g shows a higher level of liquefaction and longer duration of strong liquefaction. In addition, the r_u kept the trend of dropping after the end of shaking and to zero within the interval between different input motions.

For the saturated medium dense sand in this study, the dilation phenomenon (shear-induced volume increase) was observed during the test, which was presented as a sharp reduction in r_u. As can be seen in Fig. 5, dilation phenomenon initially occurred at the transient stage (i.e., the moment that r_u begins to develop). Then, it took place intermittently at the duration of strong liquefaction. By comparison between P2/P3 and P4, the dilation phenomenon was more readily observed in locations with higher level of liquefaction.

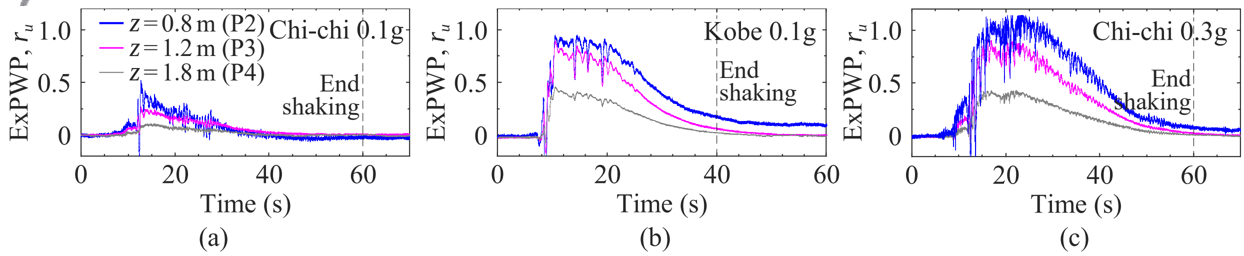

Fig. 4 – Excess pore water pressure ratio during shakings: (a) Chi-chi 0.1g, (b) Kobe 0.1g and (c) Chi-chi 0.3g.

3.3. Structural Response

3.3.1. Acceleration Response

Fig. 5 shows the comparison on time histories of superstructure acceleration between the liquefiable and nonliquefiable scenarios. The time histories of r_u and input motions were plotted together for explanation. In general, the superstructure of bridge model in liquefiable soil displayed lower maximum acceleration response compared with that in nonliquefiable soil. Combined with the development of r_u, it can be found that the superstructure acceleration in liquefiable scenarios was much lower than that in nonliquefiable scenarios since the r_u was triggered, especially in the Chi-chi 0.3g case where a significant liquefaction occurred. Also, dilation moments in the development of *ru* coincided well with the peaks of the superstructure acceleration. Besides, it was observed directly from the time histories that the liquefiable scenarios exhibited elongated acceleration response compared with the nonliquefiable scenarios, which means that the predominant frequencies of the bridge models in liquefiable scenarios were reduced.

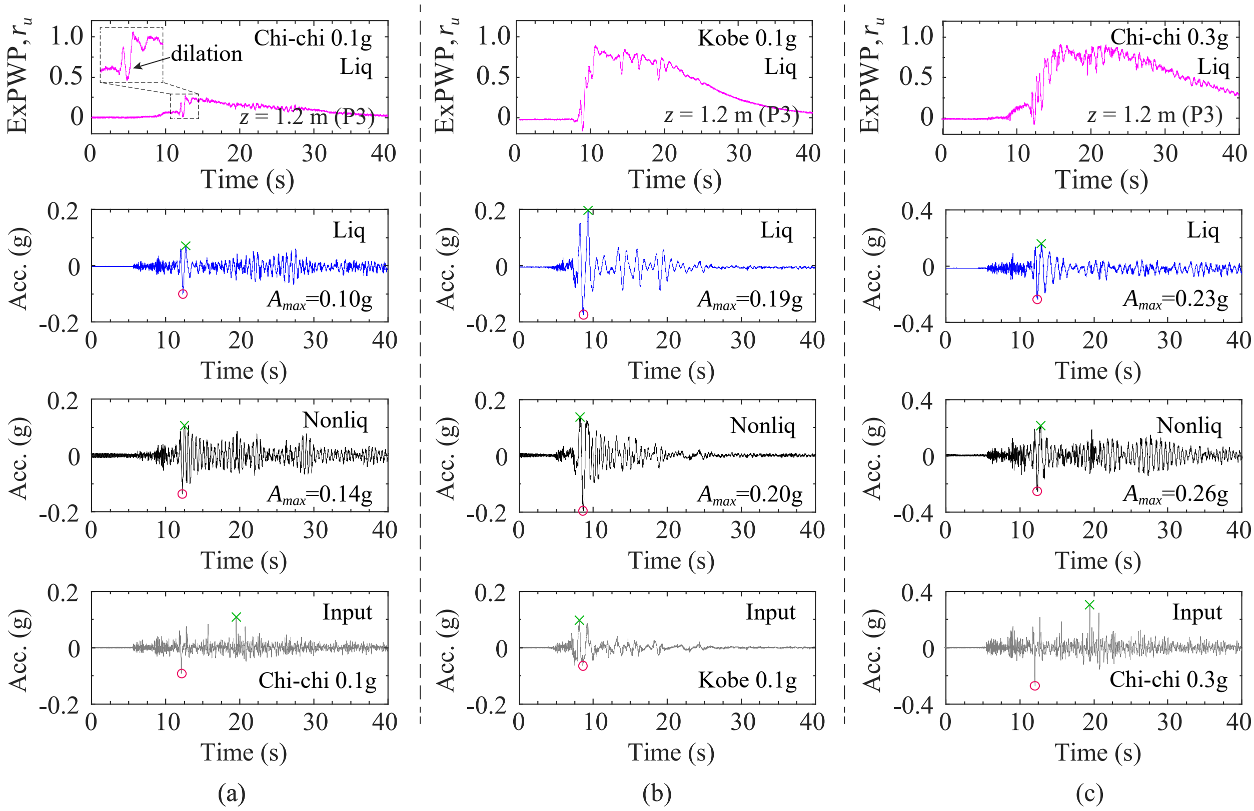

Fig. 5 – Comparison of superstructure acceleration time histories at A11 between liquefiable and nonliquefiable scenarios: (a) Chi-chi 0.1g, (b) Kobe 0.1g and (c) Chi-chi 0.3g. Symbol '○' and '×' denote the maximum negative and positive time, respectively.

3.3.2. Sectional Curvature Distribution

To reveal the seismic failure mechanism, Fig. 6 shows comparison on envelopes of curvature profiles along depth between the liquefiable and nonliquefiable scenarios. For conciseness, only the pile with the maximum curvature distribution among the 4-pile group was exhibited while the pier curvature profile was not displayed because recorded data showed that the pier practically remained elastic state during the whole tests. Note that several strain gauges were damaged during the concrete casting procedure or testing process. Fig. 6 clearly exhibits the potential yielding locations below the soil surface; that is a deeper depth-to-maximum-curvature for piles in liquefiable scenarios (6~8*D*) than that for nonliquefiable scenarios (4~5*D*) because the reduced soil resistance in liquefied scenario required a larger depth to accumulate load contribution from the soil to trigger the maximum curvature of the pile and migrated the depth-to-maximum-curvature aloof from the soil surface. Besides, the piles in liquefiable soil displayed a larger curvature at the top than underground, whereas piles in nonliquefiable soil showed reversed results. Although the curvature envelopes in Fig. 6 practically remained in elastic state (except for the pile top curvature derived from linear potentiometers in the case of liquefiable Kobe 0.1g), it is reasonably to speculate that under a scour depth of 4*D* in this study, piles in liquefiable soil may yield first at the top (i.e., pile-cap connection) while piles in nonliquefiable soil may yield first underground with a depth of 4~5*D*.

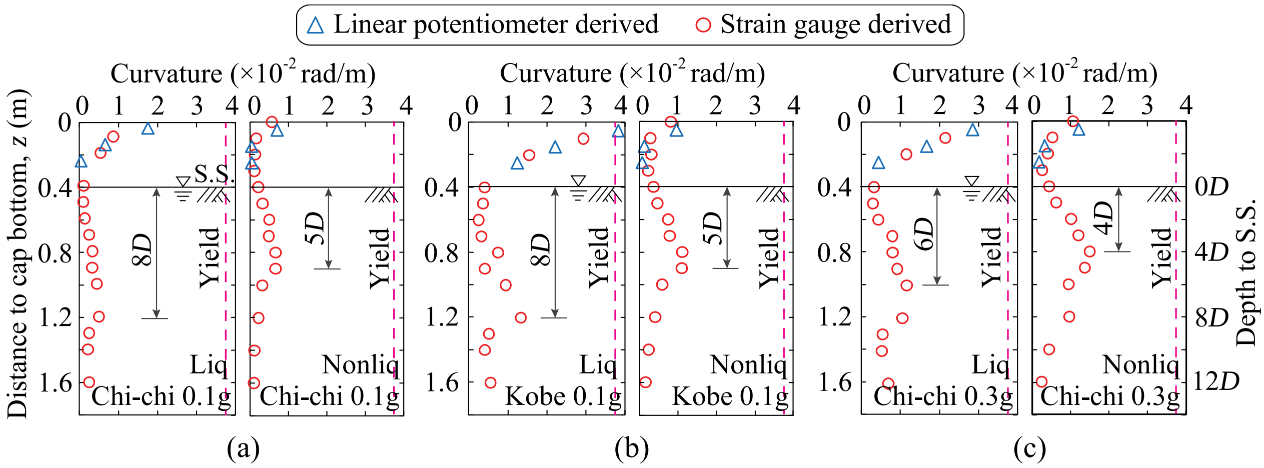

Fig. 6 – Comparison of curvature envelope distribution along depth between liquefiable and nonliquefiable scenarios: (a) Chi-chi 0.1g, (b) Kobe 0.1g and (c) Chi-chi 0.3g.

To assess the pile group effect on the seismic demands of the specimens, Fig. 7 shows the comparison on the curvature distribution between two piles at the same epoch of maximum input acceleration of the Chi-chi 0.3g case for both liquefiable and nonliquefiable scenarios. Pile A and B in Fig. 7 indicate the two piles in different rows along the excitation direction. From a quick inspection of Fig. 7 (a), it can be clearly seen that, in the nonliquefiable scenario, two piles of the group foundation showed obvious differences on the underground curvature at the same epoch. For example, the maximum underground curvature of Pile A reached approximate 0.015 rad/m while that of Pile B was relatively quite small (approximately less than 20% of Pile A). This is because of the pile group effect for the nonliquefiable scenario. In other words, soil-pile interactions on the two recorded piles were quite different. However, in the liquefiable scenario, very close curvature demands for the two piles were observed along the pile length, which indicates that a relative low level of pile group effect exists in the liquefiable scenario. In other words, the soil-pile interactions on Pile A and B are very similar. This observation is consistent with the previous study by Rollins et al. [20]; that is an in-site experimental study on the seismic responses of pile groups in soils with blast-induced liquefaction.

To quantify the seismic failure mechanism of pile groups in liquefiable or nonliquefiable scenarios, Fig. 8 and 9 illustrate time histories of pile curvature at pile top derived from linear potentiometers (z = 0.05 m) and at underground locations with maximum response derived from strain gauges (z = 1.0 or 0.9 m) for the final shakings, i.e., Kobe 0.3g and Chi-chi 1.0g for the liquefiable and nonliquefiable scenarios, respectively. As can be seen in Fig. 8(a) and (b) for the liquefiable scenario, the pile top section yielded earlier than the underground

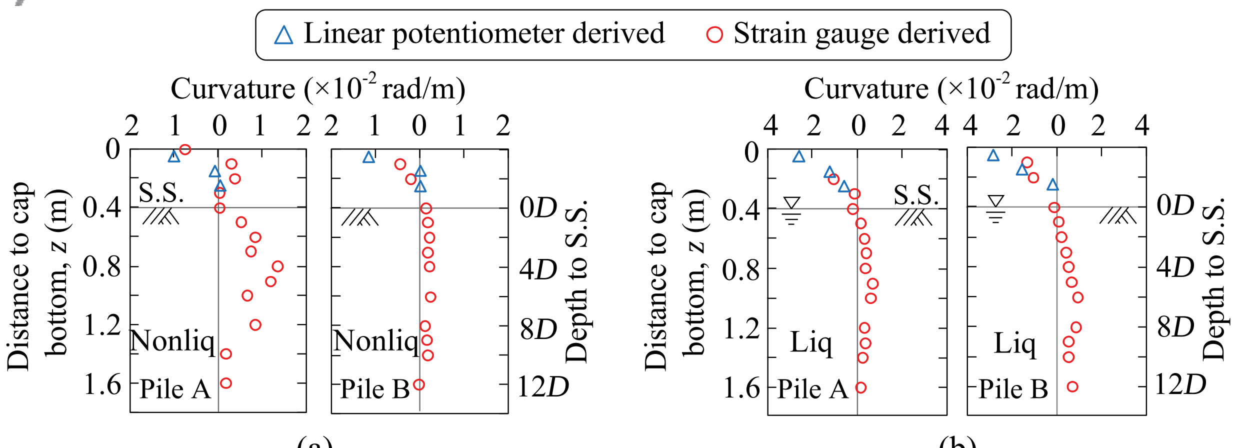

Fig. 7 – Comparison of curvature distribution along depth for two piles at the maximum acceleration epoch of Chi-chi 0.3g between (a) nonliquefiable scenario and (b) liquefiable scenario

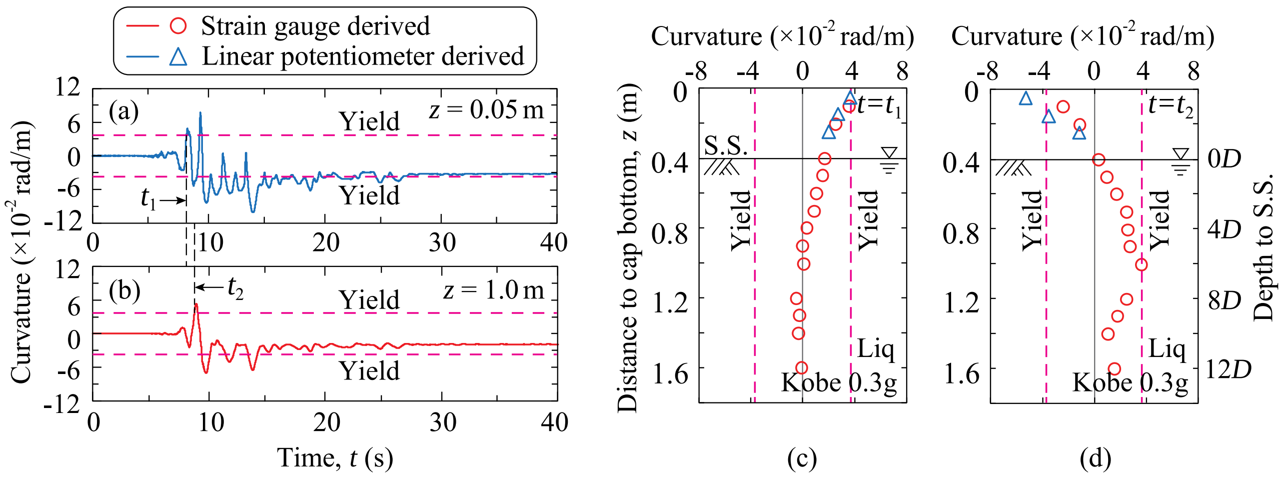

Fig. 8 – Curvature response for liquefiable scenario under Kobe 0.3g: (a) time history of pile head, (b) recorded maximum time history of underground pile, (c) distribution along depth at t_1 and (d) distribution at t_2.

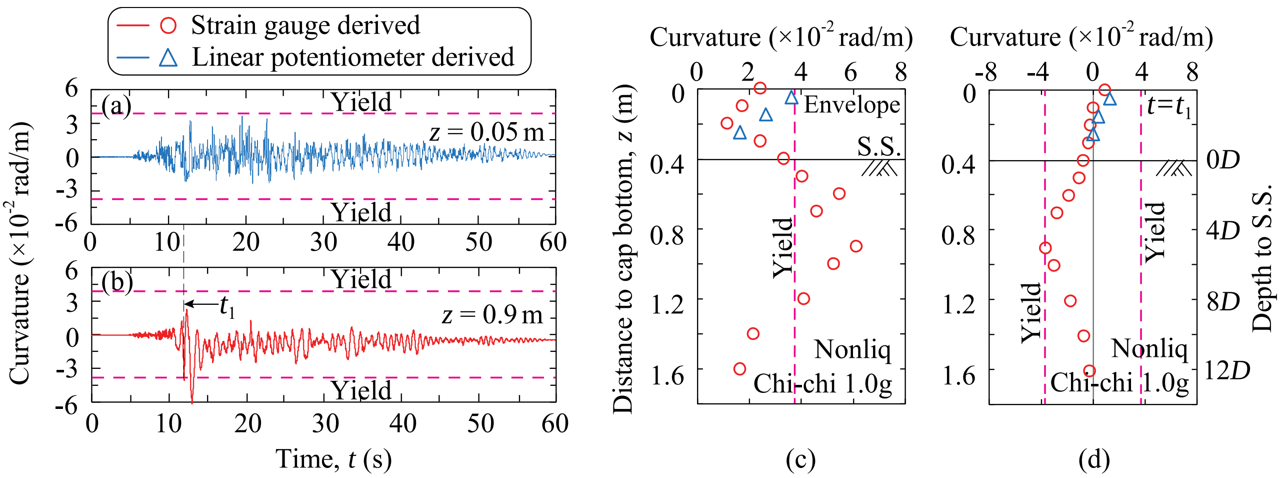

Fig. 9 – Curvature response for nonliquefiable scenario under Chi-chi 1.0g: (a) time history of pile head, (b) recorded maximum time history of underground pile, (c) envelope distribution and (d) distribution at t_1.

pile (t_1<t_2). Correspondingly, the curvature distributions at t_1 and t_2 were plotted in Fig. 8(c) and (d), respectively. Clearly, when the pile top firstly yielded at the time of t_1, low curvature was triggered at underground piles, while the pile top entered into inelastic state when the underground pile firstly suffered yielding at t_2.

Fig. 9 indicates a different failure process for the bridge model in the non-liquefiable scenario. The time history of curvature at the pile top section derived from linear potentiometers in Fig. 9(a) indicates that the pile top section kept in elastic state. However, the underground pile suffered yielding at t_1 (Fig. 9(b)). In further, an envelope distribution in Fig. 9(c) confirmed the apparent yielding of underground pile and almost elastic response of the aboveground pile. Note that the strain gauge derived curvature at the pile top section remained in elastic state distinctly. Also, the curvature distribution at the epoch of t_1 was plotted in Fig. 9(d) where the underground pile firstly yielded, whereas the pile top section was far from yielding at that epoch.

In summary, it can be concluded that, for bridge structures under a scour depth of 4*D*, two plastic regions may be formed on pile head and underground successively in liquefiable soil under strong seismic excitation. By contrast, an underground plastic region is formed first for the bridge structures in nonliquefiable soil. The plastic region at pile head may be formed later under strong ground motion. It is worth to note that under other scour depths, the seismic failure mechanism of the bridge model may be quite different from that in this study. More tests or numerical analysis are required to explicate this issue.

3.4. Post-Test Physical Observation

Post-test physical observations of the damaged bridge models supported the measured structural curvature response. As can be seen in Fig. 10, for the liquefiable scenario, 2*D*-height damaged regions of the aboveground piles were exhibited with readily observed horizontal cracks. The underground piles formed dense horizontal cracks (5 cm interval) at the depth from 2*D* to 10*D* to the soil surface, implying that the depth-to-maximum-curvature was around 6*D*, which coincided to the curvature distribution for liquefiable scenario in Fig. 6(c). No obvious cracks were detected on the pier bottom. As to the nonliquefiable scenario displayed in Fig. 10(b), neither the aboveground piles nor the pier formed obvious cracks. Main damage regions with dense horizontal cracks (5 cm interval) were located at a depth from *D* to 7*D* to the soil surface. The 6*D*-length region coincided well with the envelope distribution of pile curvature in Fig. 9(c).

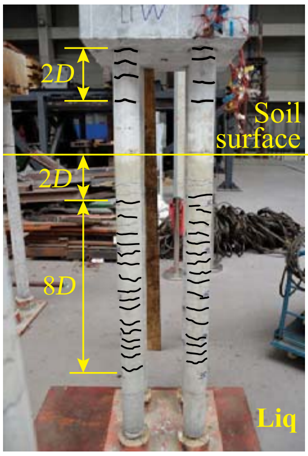

(a)

(b)

Fig. 10 – Physical observation of post-test damage features for bridge models in: (a) liquefiable and (b) nonliquefiable scenarios

4. Concluding Remarks

A series of shaking table tests were carried out to investigate the seismic response and failure mechanism of pile-supported bridge models partially embedded in a scoured ground with or without liquefiable soil. Test results indicate that the soil-bridge system in liquefiable ground showed lower frequencies and higher damping ratios in both soil and structure compared with that in the nonliquefiable ground. Besides, the high level of liquefaction can reduce the shear modulus of soil and de-amplify the peak acceleration in the wave propagation process. In general, a strong effect of soil liquefaction on the seismic failure mechanism of pile-supported bridges under scour scenario of 4*D* depth; that is two plastic regions were formed on pile head and underground successively for bridges in liquefiable soil. By contrast, the underground plastic region was formed first for bridges in nonliquefiable soil. Also, bridge pile foundations in liquefiable sand displays a deeper depth of underground plastic region than that in nonliquefiable sand.

5. Acknowledgements

This work is supported by the National Natural Science Foundation of China (Grant No. 51278375) and the Key Laboratory of Disaster Reduction in Civil Engineering, Ministry of Science and Technology of China (Grant No. SLDRCE 15-B-05). All staffs in the Multi-Functional Shaking Table Lab of Tongji University are greatly acknowledged, especially Drs. Yan Xu, Chengyu Yang and Jianzhong Li, who provide lots of insightful suggestions to our experiments. Special thanks to the RAMSIS Lab in Ohio State University for providing the first author with facilities and tools to complete this paper.

6. Copyrights

7. References

[1] Bray, J., Frost, D. and others. (2010) Geo-engineering reconnaissance of the 2010 Maule, Chile earthquake. *Report No GEER-022 of the NSF Sponsored GEER Association Team*, **1**.

[2] Maurer, B.W., Green, R.A., Cubrinovski, M. and Bradley, B.A. (2014) Evaluation of the liquefaction potential index for assessing liquefaction hazard in Christchurch, New Zealand. *Journal of Geotechnical and Geoenvironmental Engineering*, **140**, 1–11. https://doi.org/10.1061/(ASCE)GT.1943-5606.0001117

[3] FHWA. (2012) Evaluating scour at bridges [Internet]. 5th editio. Arneson LA, Zevenbergen LW, Lagasse PF, and Clopper PE, editors. U.S. Department of Transportation, Washington, DC.

[4] Wang, X., Ye, A., He, Z. and Shang, Y. (2016) Quasi-static cyclic testing of elevated RC pile-cap foundation for bridge structures. *Journal of Bridge Engineering*, **21**, 4015042. https://doi.org/10.1061/(ASCE)BE.1943-5592.0000797.

[5] Melville, B.W. and Coleman, S.E. (2000) Bridge scour. Water Resources Publication, Highlands Ranch, CO.

[6] Liu, L. and Dobry, R. (1995) Effect of liquefaction on lateral response of piles by centriguge model tests. *NCEER Bulletin*, 7–11.

[7] Brandenberg, S.J., Boulanger, R.W., Kutter, B.L. and Chang, D. (2005) Behavior of Pile Foundations in Laterally Spreading Ground during Centrifuge Tests. *Journal of Geotechnical and Geoenvironmental Engineering*, **131**, 1378–91. https://doi.org/10.1061/(ASCE)1090-0241(2005)131:11(1378)

[8] Bhattacharya, S. (2003) Pile instability during earthquake [phdthesis]. University of Cambridge.

[9] Dungca, J.R., Kuwano, J., Takahashi, A., Saruwatari, T., Izawa, J., Suzuki, H. et al. (2006) Shaking table tests on the lateral response of a pile buried in liquefied sand. *Soil Dynamics and Earthquake Engineering*, **26**, 287–95. https://doi.org/10.1016/j.soildyn.2005.02.021

[10] Tang, L. and Ling, X. (2014) Response of a RC pile group in liquefiable soil: A shake-table investigation. *Soil Dynamics and Earthquake Engineering*, **67**, 301–15. https://doi.org/10.1016/j.soildyn.2014.10.015

[11] Weaver, T.J., Ashford, S.A. and Rollins, K.M. (2005) Response of 0.6 m Cast-in-Steel-Shell Pile in Liquefied Soil under Lateral Loading. *Journal of Geotechnical and Geoenvironmental Engineering*, **131**, 94–102. https://doi.org/10.1061/(ASCE)1090-0241(2005)131:1(94)

[12] Ashford, S.A., Juirnarongrit, T., Sugano, T. and Hamada, M. (2006) Soil–Pile Response to Blast-Induced Lateral Spreading. I: Field Test. *Journal of Geotechnical and Geoenvironmental Engineering*, **132**, 152–62. https://doi.org/10.1061/(ASCE)1090-0241(2006)132:2(152)

[13] Wang, S.-C., Liu, K.-Y., Chen, C.-H. and Chang, K.-C. (2015) Experimental investigation on seismic behavior of scoured bridge pier with pile foundation. *Earthquake Engineering and Structural Dynamics*, **44**, 849–64. https://doi.org/10.1002/eqe.2489

[14] AASHTO. (2012) AASHTO LRFD bridge design specifications. 6th ed. American Association of State Highway and Transportation Officials, Washington, DC.

[15] Aviram, A., Aviram, A., Mackie, K., Mackie, K., Stojadinovic, B. and Stojadinovic, B. (2008) Guidelines of nonlinear analysis of bridge structures in California. PEER Rep. Pacific Earthquake Engineering Research Center, Berkeley, CA.

[16] Fleming, K., Weltman, A., Randolph, M. and Elson, K. (2008) Piling engineering. CRC press.

[17] McKenna, F., Scott, M.H. and Fenves, G.L. (2010) Nonlinear finite-element analysis software architecture using object composition. *Journal of Computing in Civil Engineering*, **24**, 95–107. https://doi.org/10.1061/(ASCE)CP.1943-5487.0000002

[18] Wu, X., Sun, L., Hu, S. and Fan, L. (2002) Development of laminar shear box used in shaking table test. *Journal of Tongji University (Natural Science)*, **30**, 781–785 (in Chinese).

[19] MathWorks. (2015) MATLAB the language of technical computing [Internet]. MathWorks. https://doi.org/10.1007/s10766-008-0082-5

[20] Rollins, K.M., Gerber, T.M., Lane, J.D. and Ashford, S.A. (2005) Lateral Resistance of a Full-Scale Pile Group in Liquefied Sand. *Journal of Geotechnical and Geoenvironmental Engineering*, **131**, 115–25. https://doi.org/10.1061/(ASCE)1090-0241(2005)131:1(115)